

Mechanical Modeling of Ultrasonic Welding

Analytical and numerical modeling of spot ultrasonic welding on thin metal foils is motivated by a new ultrasonic rapid prototyping technology

BY C. DOUMANIDIS AND Y. GAO

ABSTRACT. This article analyzes the mechanics of the metal ultrasonic welding process as a basis for a new solid free-form fabrication technology. Three-dimensional prototypes are constructed by ultrasonic welding of overlaid metal foil laminations, followed by contour cutting of the 2-D layers. This was implemented in the laboratory by a computer-automated ultrasonic welding station, and the normal compression, ultrasonic vibration, and process time for a single weld were experimentally optimized. The layered prototypes from aluminum foil exhibit density and stiffness comparable to solid specimens. Using strain gauge measurements on the prototype surface, the friction conditions at the foil-substrate interface were characterized via a simple analytical model of the elastic stress field and used to calibrate a full numerical simulation of the ultrasonic welding mechanics in order to relate the propagation of plastic deformation to the bond development. Besides solid metal and multi-material composites, “cold” ultrasonic welding enables integration of prefabricated components into intelligent structures, yielding active prototypes with internal functionality.

Introduction

Fusion welding methods have been pivotal for an important class of solid free-form fabrication (SFF) technologies based on molten metal transfer. These include shape deposition manufacturing (Ref. 1), shape melting technology (Ref. 2), direct metal deposition (Ref. 3), 3-D welding (Ref. 4), electron beam SFF (Ref. 5), SFF by gas metal arc welding (GMAW, Ref. 6), scan welding (Ref. 7), and other methods. However, fusion welding based SFF methods exhibit several limitations related to the molten material deposition. In particular, use of metal fusion may result in solidification defects (porosity, inclusions, incomplete fusion, columnar and segregated structures, etc.) and undesirable material transformations (sensitization, softening, embrittlement, etc.). Fu-

sion welding techniques are usually not well suited to welding of dissimilar metals or incorporation of various other materials to metal-matrix composite (MMC) structures. Moreover, the elevated welding temperatures and the associated differential thermal expansion and contraction often result in residual stresses and/or thermal distortions, compromising the dimensional tolerances and size of parts that can be built. These deficiencies, as well as certain inherent health and safety hazards (burns, electric shocks, toxic fumes, irradiation, etc.) hinder a wider commercialization of these technologies.

These limitations of fusion welding in SFF processes are addressed by the ultrasonic rapid prototyping (URP) technology (Ref. 8). This is based on ultrasonic welding (USW) of thin material foil on the stack of previously joined layers, followed by contour cutting (e.g., carbide tip scribing) to blank the proper foil section. This laminated part fabrication reaps the benefits of the USW process for simple, efficient, safe, solid-state “cold” joining of multiple materials, as well as its scalability and integration capability in rapid prototyping procedures. Therefore, the objectives of this article are to elaborate on the laboratory implementation of spot ultrasonic welding of thin metal foils and the selection and optimization of the process conditions for URP. For this purpose, however, the main emphasis in this paper is on the development, calibration, and validation of a USW mechanical model using numerical, analytical, and experimental methods, and its utilization for studying the welding features in URP.

Ultrasonic welding is a solid-state joining process producing a bond by local high-frequency (f) vibration of amplitude X , coupled with normal compression P of the parts for a short time period T — Fig. 1 (Ref. 9). Empirical studies of the USW

process mechanisms and the resulting material microstructures (Refs. 10–13), the ultrasonic weldability of metallic and other materials (Refs. 14–18), and the advantages and applications of the USW method (Refs. 19–25) have been reported in the literature. This was accompanied by early research on the USW mechanics by analytical and experimental methods, including photoelasticity and microscopy (Refs. 10–13, 26, 27), and on heat transfer by analytical and calorimetric techniques, particularly in the former-Soviet literature (Refs. 27–29). Newer works in the bibliography address USW process monitoring, control, and optimization (Refs. 29, 30), precision joining (Refs. 31, 32), and new technologies, especially in Japan (Ref. 17). However, there is still an outstanding need for comprehensive and quantitative description of the USW mechanisms, to enable new process applications such as in rapid prototyping.

Laboratory Implementation

Thus, ultrasonic welding offers an ideal basis for solid free-form fabrication of objects from multiple material foils and other elements. The arrangement of such ultrasonic rapid prototyping is illustrated in Fig. 2. The prototype materials are fed in thin foil form from a supply drum to the process table. The layered part is built on an anvil base driven by the positioning table, with the new foil fed at the top of the stack. This is welded by the sonotrode tip or wheel to the already deposited layers, through multiple ultrasonic spot or seam welds, forming a grid inside the welded foil section. The sonotrode is surrounded by a clamping fixture, compressing vertically and constraining the welded layers in place, to damp out the stress waves and protect the previous welds against potential resonances. For parts with overhanging regions, these are supported by an auxiliary sacrificial material envelope surrounding the prototype within a retractable wall fixture. Next, the top layer is cut to the proper section contours by fine end milling or diamond/carbide tip scribing. The regions of the surrounding support envelope are also crosshatched during each machining step for easy removal after the end of the process. The remaining residual portion of the top foil is re-

KEYWORDS

Ultrasonic Welding
Rapid Prototyping
Solid Free-Form Fabrication
Finite Element Analysis
Surface Friction
Aluminum Foil

C. DOUMANIDIS is with the Department of Mechanical and Manufacturing Engineering, University of Cyprus, Nicosia, Cyprus. Y. GAO is with the Department of Mechanical Engineering, Tufts University, Medford, Mass.

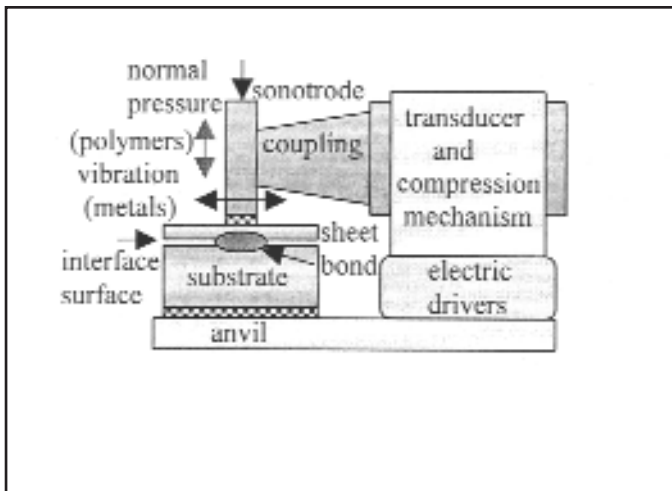


Fig. 1 — Ultrasonic welding process setup.

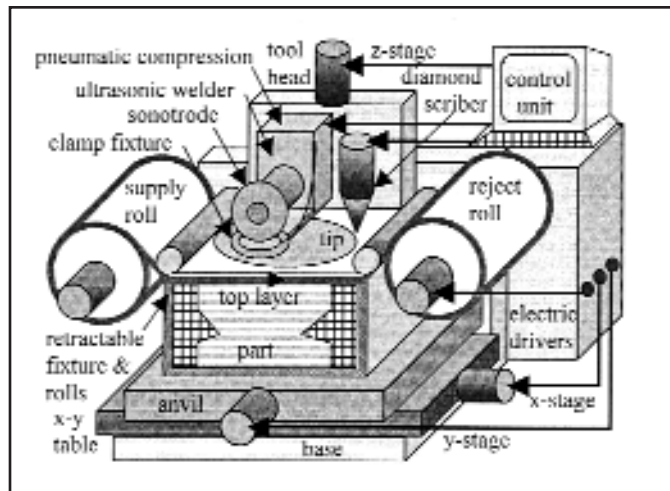


Fig. 2 — Ultrasonic rapid prototyping arrangement.

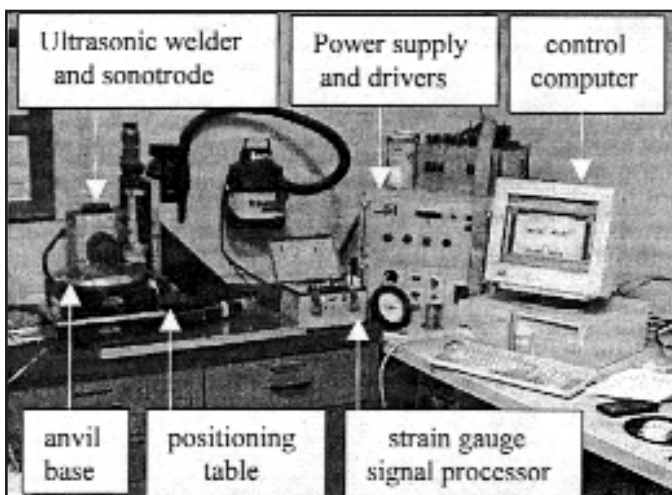


Fig. 3 — Laboratory station for ultrasonic rapid prototyping and strain gauge measurement.

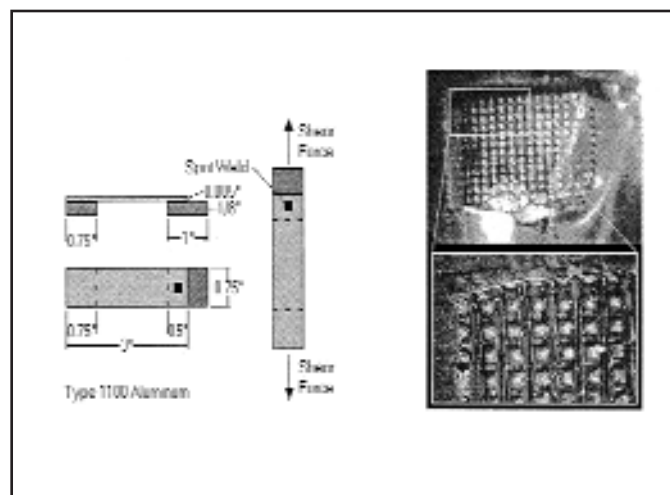


Fig. 4 — Single-weld specimens for shear tests and ultrasonic weld top view with tearing at edge.

moved after each layer processing to a recycling drum. The motion of the foil drums, the base x-y table, and the tool head z stage is coordinated through their electronic drivers by the system computer under software control.

This URP process was implemented in the laboratory on the semiautomated hardware setup of Fig. 3 (with manual material feed). This consists of a metal ultrasonic welding machine, rated at 3.5 kW and frequency $f=20$ kHz, with a 140-mm beam tool-steel sonotrode, ending at a 4 × 4-mm-square tip with textured surface. The vertical compression P is effected by six pneumatic cylinders, and the horizontal vibration amplitude X is adjustable at the transducer irrespective of the load. Cutting is performed by a fine four-flute end mill (1.59 mm in diameter) rotated by a vertical drill spindle with a speed of 5000–30,000 rpm. The anvil, consisting of

a roughened tool-steel base, as well as the tool head carrying the ultrasonic welding machine and cutting tool, are moved by stepper motor positioning stages, with optical encoder feedback and microstepping control, providing 230-mm travel and 12.7- μ m resolution. These are guided by electronic drivers through a three-axis motion control card installed in the system computer, which also controls the power units of the rotary drill press and the metal ultrasonic welding machine. The latter can be interchanged with an available plastic foil ultrasonic welding system rated at 300 W and $f=70$ kHz (not shown in Fig. 3).

The URP system software drives the hardware motions and welding/cutting operations as dictated by the prototype geometry to be constructed. This is imported in standard structural triangle language (STL) computer-aided design (CAD) format, in which the external sur-

face of the 3-D object is represented by small triangular facets. The software routine determines the successive foil contours through sectioning these STL facets by a stack of horizontal planes corresponding to the prototype layers. The straight-line segments resulting from the triangle/plane intersections comprise the contours profile of each layer, thus defining the respective cutting tool path. For geometric precision of the machined surface, continuous-path motion along the contours is implemented during foil cutting. In ultrasonic spot welding, the weld locations are selected at the nodes of a square virtual grid superposed over the welded foil section. If the grid spacing between neighboring selected spot welds is less than the sonotrode tip size (4 mm), the adjacent or overlapping welds result in a fully welded layer area (typically used for aluminum prototypes). A fast point-to-

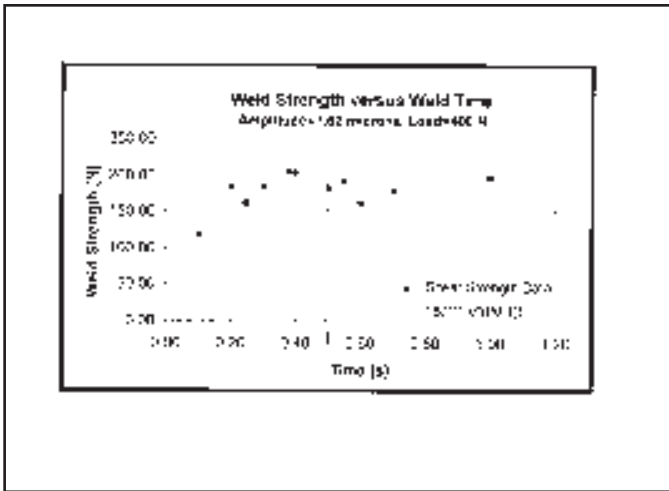


Fig. 5 — Optimization of process cycle time T through shear strength tests of single welds.

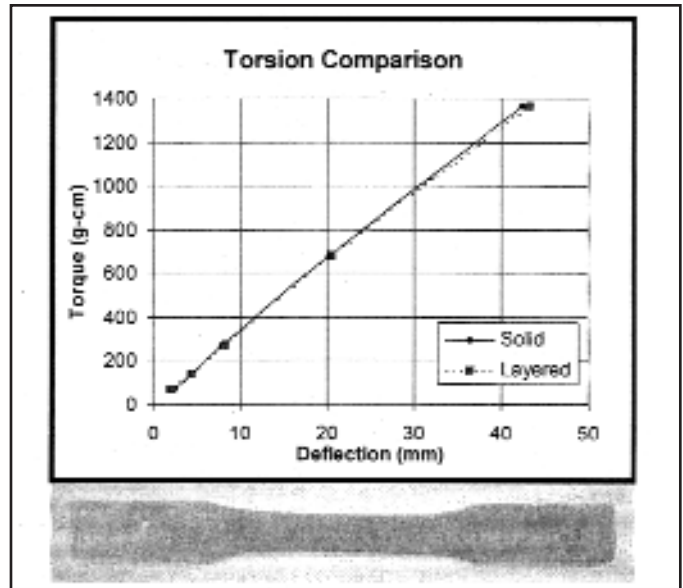


Fig. 6 — Comparative torsion test of solid and layered specimen (bottom picture).

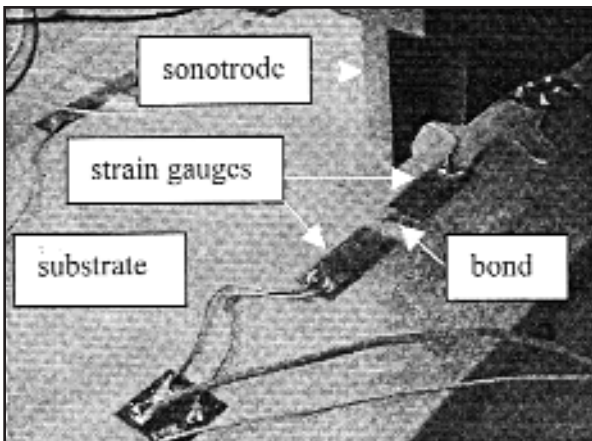


Fig. 7 — Strain gauge arrangement on substrate surface.

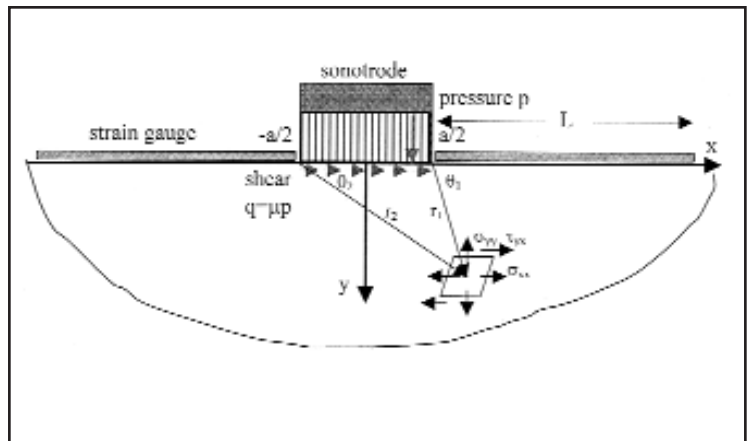


Fig. 8 — Arrangement of 2-D elastic analytical model.

point motion is used between successive spot positions. The functions of the URP system software are controlled through a graphical user interface (GUI) environment on the station computer, where all respective processing parameters are also entered and adjusted.

Process Conditions and Experimental Tests

This laboratory URP station was applied to construction of solid aluminum prototypes built from 0.127-mm-thick Al foil (1100). First, the ultrasonic welding process conditions were experimentally selected to optimize the shear strength of single lap welds on the specimens of Fig. 4 during a series of tensile tests on a universal testing machine. Thus, the normal

compression was set to $P=400$ N, the vibration amplitude to $X=7.62\ \mu\text{m}$, and the total welding cycle time to $T=0.5$ s. For example, Fig. 5 illustrates the laboratory data on maximum shear of ultrasonic welds performed at the optimal compression P and vibration X settings above, at various processing times T . It appears that after the initial increase during the weld development, the shear strength reaches its maximum value at the selected optimal cycle time $T=0.5$ s. After these optimal process conditions are exceeded, the weld region reaches the strength of the base material foil. Therefore, it is the latter, not the ultrasonic weld, that fails in tearing during the specimen tests at the stress concentration locations, i.e., the weld corners of the sonotrode tip footprint — Fig. 4. Similarly, the end-milling variables were

experimentally optimized to obtain good surface finish with minimal burr. The rotation speed was set to 30,000 rpm, the machining feed rate to 25.4 mm/s, and the depth of cut to 0.127 mm, i.e., the thickness of one aluminum foil.

Next, these process conditions were employed in fabrication of test prototypes with a dog bone geometry according to Standard ASTM E8-96a, for assessing the mechanical properties of the layered material. Figure 6 shows such a laminated aluminum specimen of 1.14-mm thickness, i.e., consisting of nine foil layers. The density of this layered prototype was found by volumetric measurements to be 98% of that of a solid aluminum specimen. Subsequently, the prototype welds were subjected to pure shear at the lamination planes during torsion tests, where the

parts are loaded to known torques by an attached 200-mm cantilever arm, thus creating angular deflections of the arm end. Figure 6 compares the torsion stiffness of the layered vs. the solid specimen, thus attesting to the mechanical integrity and strength of the layered URP prototypes. Similar results for the elastic properties of the two parts have been obtained in tension and bending experiments (Ref. 33).

Besides these eventual in-service mechanical properties of the produced URP parts, the in-process generated load and deformation distributions in the material during USW are of decisive importance for the prototype quality and its resulting performance. Therefore, as mentioned at the introduction, these are the focus of the subsequent analysis. In the laboratory, such strain in the weld region during ultrasonic welding was measured by miniature resistive gauges attached adhesively on the top surface of the already welded partial prototype (the substrate), i.e., before the top foil is welded on it. Since the experimental evidence of Fig. 4 indicates a stress concentration at the loading edges, a pair of identical strain gauges (EA-series at 350 Ω) was placed directly anterior and posterior to the sonotrode footprint area, longitudinally along the x-direction of ultrasonic vibration — Fig. 7. The strain gauges were connected in a half Wheatstone bridge to an analog power/conditioner unit for transducer excitation and signal isolation, amplification, filtering, and linearization — Fig. 3. The voltage signal was measured by an analog-to-digital data acquisition board at a frequency of 200 kHz (i.e., 10 samples per ultrasonic vibration period) and a 12-bit resolution (i.e., 2.44 mV within a 0–10 V range), and recorded by the system computer through instrumentation control software. The measured longitudinal strain ϵ_{xx} at the previously selected process conditions exhibits a sinusoidal waveform:

$$\begin{aligned} \epsilon_{xx}(t) &= \hat{\epsilon}_{xx}(t) \sin \omega t \\ \omega &= 2\pi f \\ (f &= 20 \text{ kHz}) \end{aligned} \quad (1)$$

with a time-variable amplitude envelope $\hat{\epsilon}_{xx}$ during the welding cycle. These laboratory data are used for identification and calibration of the frictional conditions at the top foil-substrate interface, and for experimental validation of the analytical and numerical USW mechanical models introduced below — Fig. 9.

Analytical Modeling and Interface Friction

Besides the substrate top surface, the stress-strain field must be studied in the prototype volume, and particularly at the

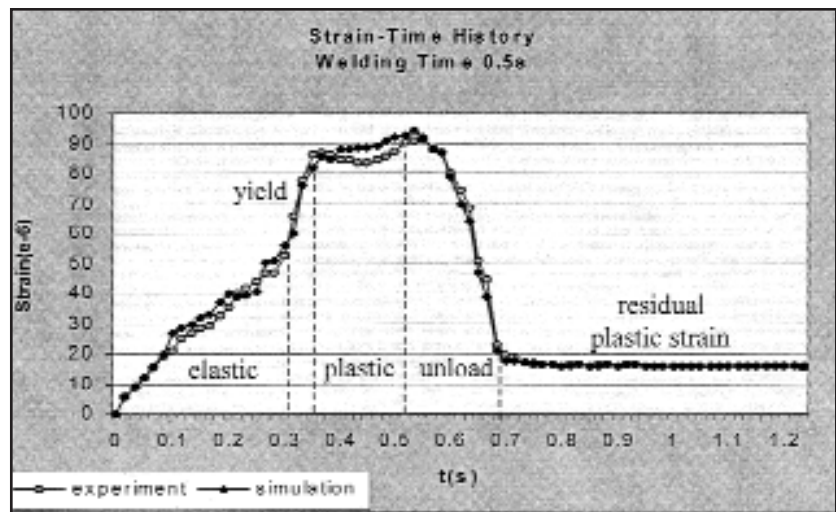


Fig. 9 — Measured and simulated surface strain amplitude during USW process cycle.

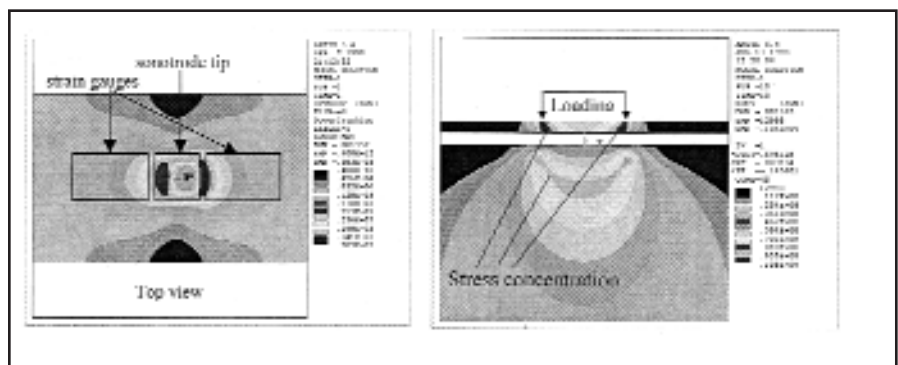


Fig. 10 — Top view and cross section of equivalent stress field at yield point.

top foil-substrate interface, where slippage occurs and the USW joint is developed. First, to obtain quantitative insights to the load and deformation distribution in the substrate, a simple analytical model of the USW process mechanics was developed (Ref. 34). This provides a static, linear elastic, two-dimensional description of the stress-strain field on a part cross section (x, y) in the direction of ultrasonic vibration — Fig. 8. In particular, the fully welded substrate material is assumed homogeneous and isotropic, with elastic properties equivalent to those of the base metal — Fig. 6. The thermal distribution during ultrasonic metal welding has been reported in the literature (Refs. 12, 35, 36) to temporarily reach peak temperatures between 35 and 65% of the material melting point (200°–400°C in aluminum). However, because of the effective heat dissipation in the aluminum sheets, as well as through the anvil and sonotrode, the temperature on the surface of the foils at the location of the strain gauges (Fig. 7) was found to reach lower levels (about

50°C at a distance of 3 mm from the sonotrode), by infrared pyrometry and thermocouple measurements (Ref. 37). Therefore, the material properties were assumed as invariant at an average temperature of 30°C. The thick substrate is approximated by an elastic half-space under plane stress conditions (i.e., with negligible stress $\sigma_{zz}=0$ in the transverse direction z , where the prototype is unconstrained). This is loaded on its free surface by a uniform normal pressure $p=P/A=25$ MPa under the sonotrode area $A=16$ mm², and a tangential shear $q=Q/A$ due to friction Q with the top foil, generating the stress distribution — Fig. 8:

$$\begin{aligned} \sigma_{xx}(x, y) = & \\ & -\frac{p}{2\pi} \left[2(\theta_1 - \theta_2) + (\sin 2\theta_1 - \sin 2\theta_2) \right] \\ & + \frac{q}{2\pi} \left[4 \ln \frac{r_1}{r_2} - (\cos 2\theta_1 - \cos 2\theta_2) \right] \end{aligned} \quad (2A)$$

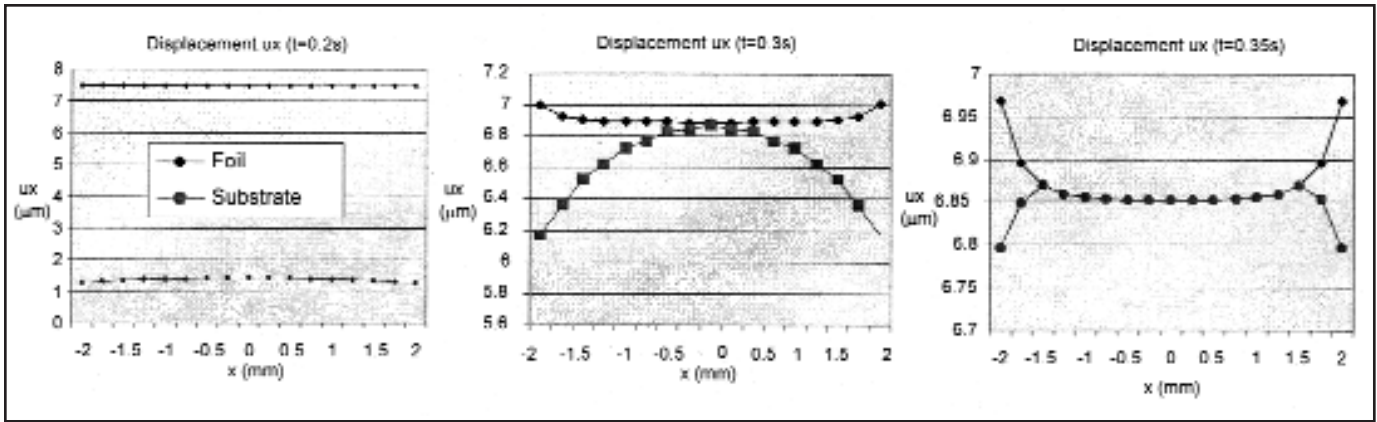


Fig. 11 — Horizontal displacement amplitude on foil and substrate contact surface under the tip.

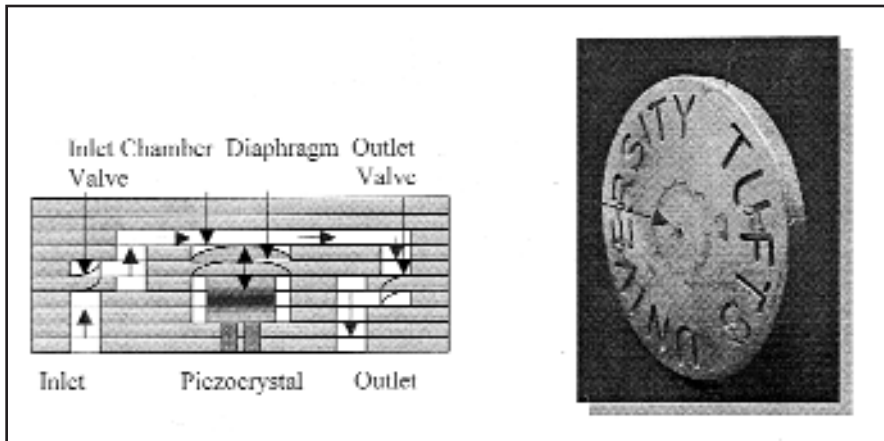


Fig. 12 — Schematic arrangement of microfluidic pump and USW aluminum prototype.

in the strain Equations 3A–C, and integrated over the strain gauge length L (Fig. 8) to yield an averaged estimate of the maximum measured strain on the surface. By comparing the resulting analytical maximum value of $\hat{\epsilon}_{xx}$ to the experimental strain amplitude data (Equation 1), the friction coefficient μ can be identified as

$$\begin{aligned} \hat{\epsilon}_{xx}(t) &= \frac{c}{E} [q(t) - vp] \\ &= \frac{c}{E} p [\mu(t) - v] \\ \Rightarrow \mu(t) &= \frac{E}{cp} \hat{\epsilon}_{xx}(t) + v \quad (4) \end{aligned}$$

where $c=1.075$ is a geometric constant, dependent on the strain gauge length (for $L=2a$). Equation 4 yields an estimate of the friction coefficient $\mu(t)$ that varies, over the time of a USW process cycle (in the range of 0.33–0.58 for Al), linearly with the surface strain measurements.

Numerical Simulation and Plastic Deformation

Beyond characterization of the friction conditions at the interface surface by the previous elastic closed-form model, a study of plastic deformation analysis in the prototype volume must be performed, in relation to the USW weld development. For this purpose, a full numerical simulation was established based on the finite element method (FEM, Ref. 40), to describe the USW process mechanics in both the top foil and the substrate. This is a dynamic, elastoplastic, three-dimensional computational model, with flexibility in the representation of complex prototype geometries, ultrasonic vibration cycles, and material properties. In particular, the energy of distortion criterion (von Mises, Ref. 38) is employed for the transition from elastic deformation to plastic yield, which occurs when the scalar equivalent

$$\begin{aligned} \sigma_{yy}(x, y) &= \\ &= -\frac{p}{2\pi} \left[2(\theta_1 - \theta_2) - (\sin 2\theta_1 - \sin 2\theta_2) \right] \\ &+ \frac{q}{2\pi} \left[\cos 2\theta_1 - \cos 2\theta_2 \right] \quad (2B) \end{aligned}$$

$$\begin{aligned} \tau_{yx}(x, y) &= \\ &= -\frac{p}{2\pi} \left[\cos 2\theta_1 - \cos 2\theta_2 \right] \\ &- \frac{q}{2\pi} \left[2(\theta_1 - \theta_2) + (\sin 2\theta_1 - \sin 2\theta_2) \right] \quad (2C) \end{aligned}$$

$$\text{where } \theta_{1,2} = \tan^{-1} \left(\frac{y}{x \mp \frac{a}{2}} \right),$$

$$r_{1,2} = \sqrt{\left(x \mp \frac{a}{2} \right)^2 + y^2},$$

and $a=4$ mm is the tip size — Fig. 8.

Clearly, the linear elastic stress field of Equations 2A–C is a superposition of two terms, due to pressure p and shear q , respectively. The respective elastic strain field for plane stress loading is (Ref. 38)

$$\begin{aligned} \epsilon_{xx}(x, y) &= \frac{1}{E} \left[\sigma_{xx}(x, y) - \nu \sigma_{yy}(x, y) \right] \\ \epsilon_{yy}(x, y) &= \frac{1}{E} \left[\sigma_{yy}(x, y) - \nu \sigma_{xx}(x, y) \right] \\ \gamma_{yx}(x, y) &= \frac{2(1+\nu)}{E} \tau_{yx}(x, y) \quad (3) \end{aligned}$$

where $E=72$ GPa is the Young's modulus and $\nu=0.33$ the Poisson's ratio of the material (Al 1100). In the USW process, dry friction (Coulomb, Ref. 39) conditions are assumed at the top foil-substrate interface surface. Thus the maximum shear q during one ultrasonic vibration period is related to the normal pressure p by $q=\pm\mu p$, where μ is an average friction coefficient over the contact area A under the sonotrode tip. Using this assumption, the stress Equations 2A–C can be substituted

stress σ_{eq} reaches the yield point σ_Y of the material (120 MPa for Al 1100):

$$\sigma_{eq} = \frac{1}{\sqrt{2}} \cdot \left[(\sigma_1 - \sigma_2)^2 + (\sigma_2 - \sigma_3)^2 + (\sigma_3 - \sigma_1)^2 \right]^{0.5} = \sigma_Y \quad (5)$$

where σ_1 , σ_2 , and σ_3 are the principal stress components. After yielding, the material is assumed to follow a kinematic bilinear strain-hardening behavior, i.e.:

$$\sigma_{eq} = \sigma_Y + B \left(\epsilon_{eq} - \frac{\sigma_Y}{E} \right) \quad (6)$$

where ϵ_{eq} is the scalar total strain and B the tangent modulus for hardening (64.5 MPa for Al).

It should be noted that in USW the speed of vibration $\dot{U}=X\omega=0.96$ m/s is much less than the stress wave propagation velocity in the material ($c_1=6300$ m/s for pressure waves and $c_2=3100$ m/s for shear waves in Al). Similarly, elemental inertial forces due to the ultrasonic acceleration are smaller compared to the material stiffness (Ref. 41). Therefore a quasi-static simulation was also implemented for computation efficiency, in which the stress/strain amplitudes are statically determined, and complete dynamic vibration periods are simulated only as needed. In the FEM model, the boundary conditions include absence of displacement at the anvil base and clamped lateral boundary, and absence of load at the free top foil surface. The contact area of the foil with the sonotrode tip is loaded in compression p and is displaced horizontally in ultrasonic vibration by $u_x=X\sin\omega t$. At the interface surface, no relative displacement (no slip) occurs when the local shear $\tau_{yx} < \mu(t)\sigma_{yy}$; when the dry friction limit $\tau_{yx} = \mu(t)\sigma_{yy}$ is reached at an interface point, the shear stress saturates and local slippage occurs between the foil and the substrate. The friction coefficient $\mu(t)$ in the numerical model is calibrated by the analytical estimate of Equation 4 according to the experimental data for $\hat{\epsilon}_{xx}$ (Equation 1).

Figure 9 compares these laboratory measurements of the interface strain amplitude $\hat{\epsilon}_{xx}$ to the respective predictions of the calibrated numerical simulation. The close agreement of this experimental transient with that of the computational model attests to the validity of the latter. First in the elastic domain, the initially slippery interface (μ around 0.33) limits the shear stress τ_{yx} that can be transferred to the substrate, and relative slippage with the top foil results in low elastic strains $\hat{\epsilon}_{xx}$.

However, as the USW friction progressively alters the tribological conditions by disruption of surface films, increase of the metallic contact area, moderate temperature rise, and establishment of micro-welds, $\mu(t)$ grows with time, gradually increasing the surface strain (Equation 4) due to the afforded higher shear stress. Figure 10 illustrates the equivalent stress field σ_{eq} (Equation 5) on the longitudinal (x,y) cross section and the top surface (x,z) of the substrate, at the end of the purely elastic regime (i.e., at about $t=0.3$ s in Fig. 9). This demonstrates the 3-D stress distribution in the part, as well as the observed stress concentration at the anterior and posterior edge of the sonotrode contact surface in the direction of ultrasonic vibration.

Next, when the latter stress level reaches the yield point at these stress concentration points (Equation 5), local plastic deformation is initiated. In this plastic regime (Fig. 9), the stress, the measured strain, and the friction coefficient show only a modest increase due to strain-hardening (Equation 6), thus allowing further metal regions to yield. As the plastically deformed zone propagates, the limited interface shear τ_{yx} at these yielded areas, in combination with the prominent interfacial friction (μ around 0.58), enforce locally the no-slip condition again. Therefore, the foil surface is attached locally to the substrate, thus resulting in the gradual development of the ultrasonic weld region. Finally, at the end phase of the USW process, the material is elastically unloaded, with some residual plastic strain remaining at the measurement region — Fig. 9.

The establishment of the joint on the interface surface is further illustrated in Fig. 11, which plots the simulated distributions of longitudinal displacement amplitude u_x for the foil and substrate surfaces under the sonotrode tip ($-a/2, a/2$). At the initial elastic deformation (at $t=0.2$ s, Fig. 11A), the gap between the displacement of the foil (almost uniformly equal to the sonotrode vibration amplitude X) and the small one of the substrate surface represents the relative slip between the two sides. Inception of plastic deformation (at $t=0.3$ s, Fig. 11B) is manifested by the large displacements of both the foil and the substrate metal, peaking at the center of the contact area. There the relative displacement gap is bridged completely and the local slippage is eliminated, thus generating the ultrasonic weld nucleus. Within a short time ($t=0.35$ s, Fig. 11C), this initial anchoring between the two sides is spread over most of their contact surface under the sonotrode tip, where their displacements are equalized and permanent attachment ensues as a re-

sult of the USW welding mechanisms mentioned before. This joining at the surface subsequently raises the stress level and leads the surrounding region inside the foil and the substrate volume into the plastic regime, as discussed above, therefore expanding the cross section of the ultrasonic weld.

Conclusion

The previous numerical simulation, with its interface boundary conditions experimentally calibrated via the analytical model, provides a flexible tool for the study of USW in rapid prototyping applications. It is presently used for further optimization of the process conditions, the sonotrode tip geometry, the configuration and spacing of the weld location grid, etc. It can also be employed for ultrasonic weldability analysis of dissimilar metal and nonmetal foils, since incompatibility of the material compliances and plasticity properties for USW can be indicated in the model predictions. The simulation is also applied for investigation of potential fatigue failure of previous joints under the cyclic loading from subsequent welds, the stress concentration, and crack propagation at the edges of unwelded interface regions. In addition, the FEM model can simulate the deformation of prototypes with complex external geometry, as well as loading of delicate components encapsulated internally in the part volume during layered fabrication. Figure 12 shows a URP-fabricated functional miniature pump prototype with internal valves, diaphragm, and external lettering, constructed of 60 aluminum foil layers.

In summary, a new rapid prototyping technology is enabled by ultrasonic welding for fabrication of functional parts with embedded active components and internal structures (such as shape memory alloys, Ref. 42), as well as custom-designed, dense, and sound-layered metal products. This method is based on the ultrasonic welding process of thin foils, combining solid-state, low-temperature, high-strength welding with the flexibility and integration capability of prefabricated elements. Toward an analysis of ultrasonic rapid prototyping, the establishment of a single metal ultrasonic weld through plastic deformation analysis was studied, using a flexible numerical simulation of the process mechanics developed in this research. The friction conditions at the foil-prototype interface surface were calibrated via a simpler analytical elastic model of the stress field during the process, using experimental data from strain gauges. The tests were run on a computer-automated ultrasonic welding station in the laboratory, in which the pro-

cessing conditions were experimentally optimized, and the fabricated layered prototypes from aluminum foil were shown to exhibit density and stiffness properties comparable to those of solid metal specimens.

Acknowledgments

This research was supported by a Honda Initiation Grant and by NSF Award DMI-9820790.

References

1. Fessler, J. R., Merz, R., Nickel, A. H., Prinz, F. B., and Weiss, L. E. 1996. Laser deposition of metals for shape deposition manufacturing. *Proc. SFF Symp.*, Austin, Tex. pp. 117-124.
2. Doyle, T. E. 1990. Shape melting technology. *Natl. Conf. on Rapid Prototyping*, Dayton, Ohio. pp. 55-62.
3. Mazumder, J., Choi, J., Nagarathnam, K., Koch, J., and Hertzner, D. 1997. The direct metal deposition of H13 tool steel for 3-D components. *JOM* 49(5): 55-60.
4. Dickens, P. M., Pridham, M. S., Cobb, R. C., Gibson, I., and Dixon, G. 1992. Rapid prototyping using 3-D welding. *Proc. Solid Freeform Fabrication Symp.*, Austin, Tex. pp. 280-290.
5. Dave, V. R., Matz, J. E., and Eagar, T. W. 1995. Electron beam solid freeform fabrication of metal parts. *Proc. Solid Freeform Fabrication Symp.*, Austin, Tex. pp. 64-71.
6. Kovacevic, R., and Kmecko, I. 2000. SFF based on controlled gas metal arc welding. *Proc. NSF Manuf. Grantees Conf.*, Vancouver, Canada.
7. Korizis, G., and Doumanidis, C. 1999. Scan welding: thermal modeling and control of material processing. *J. of Manuf. Science & Eng. Trans. ASME* 121(3): 417-424.
8. Johnson, N., Gao, Y., and Doumanidis, C. 2000. Multi-material rapid prototyping by ultrasonic welding. *Proc. 3rd World Congress on Intel. Manuf. Proc. & Systems*, CIRP, Cambridge, Mass. pp. 230-237.
9. Jellison, J. L., Albright, C. E., Devine, J., Harmon, G., Knorovsky, G. A., Winchell II, V. H., and Papritan, J. C. 1991. Ultrasonic welding. *Welding Handbook* Ch. 25, 8th edition, O'Brien, R. L., ed. Miami, Fla.: American Welding Society.
10. Devine, J. 1984. Joining metals with ultrasonic welding. *Machine Design* 56(21): 91-95.
11. Jones, J. B. 1961. Phenomenological considerations in ultrasonic welding. *Welding Journal* 40(4): 289-s to 305-s.
12. Hazlett, T. H., and Ambekar, S. M. 1970. Additional studies of interface temperature and bonding mechanisms of ultrasonic welds. *Welding Journal* 49(5): 196-s to 200-s.
13. Kirzanowski, J. E. 1989. A TEM study of ultrasonic wire bonding. *Proc. 39th IEEE Electronic Component Conf.*, Houston, Tex. pp. 450-455.
14. Flood, G. 1997. Ultrasonic energy welds copper to aluminum. *Welding Journal* 76(1): 43-45.

15. Shin, S., and Gensoy, H. T. 1968. Ultrasonic welding of metals to nonmetallic materials. *Welding Journal* 49(9): 398-s to 403-s.
16. Ramarathnam, G., Libertucci, M., and Sadowski, M. M. 1992. Joining of polymers to metal. *Welding Journal* 71(12): 483-s to 490-s.
17. Tsujino, J., Ueoka, T., and Hasegawa, K. 1996. New methods of ultrasonic welding of metal and plastic materials. *Ultrasonics* 34(2-5): 177-185.
18. Matsuoka, S. 1998. Ultrasonic welding of ceramics/metals. *J. of Material Process Technology* 75(1-3): 259-265.
19. Damongeot, A., and Andre, G. 1988. Noise from ultrasonic welding machines — risks and prevention. *Applied Acoustics* 25(1): 49-66.
20. Mazur, A. I., Aleshech, V. G., and Shorshor, M. K. 1974. Improving quality of ultrasonic welding of metal to semiconductors. *Automated Welding* 27(1): 66-68.
21. Meyer, F. R. 1976. Assembling electronic devices by ultrasonic welding. *Electronic Packaging and Production* 16(7): 27-29.
22. Hafstrom, J. W., Killpatrick, D. H., and Niemann, R. C. 1977. Joining NBT superconductors by ultrasonic welding. *IEEE Trans. Magn.* 13(1): 94-96.
23. Richter, J., and Neumann, A. 1979. Osteosynthesis by ultrasonic welding. *ZBL Chirurg.* 104(18): 1170-1175.
24. Kuhne, W., Richter, J., and Martens, H. 1983. Wound-healing of spleen ruptures by ultrasonic welding in animal experiments. *Exper. Pathology-JENA* 24(2-3): 167-170.
25. Mikus, E. 1990. Animal experimental study with ultrasonic welding by liver cuts. *ZBL Chirurg.* 115(3): 175-180.
26. Harman, G. G., and Keedy, K. O. 1972. An experimental model of the microelectronic ultrasonic wire bonding mechanism. *10th Annual Proc. Reliability Physics*, Las Vegas, Nev. pp. 49-56.
27. Grachev, A. A., and Koptenko, V. M. 1974. Effect of mechanical properties of substances and their preparation for ultrasonic welding, on quality joints between wire and films. *Automated Welding* 27(11): 48-52.
28. Kulemin, A. V., and Kholopov, Y. V. 1980. Calculation and research into the generation of heat during the ultrasonic welding of metals. *Automated Welding* 33(2): 15-17.
29. Mazur, A. I., and Musabekov, T. Y. 1976. Control of joint quality during its formation in ultrasonic welding. *Welding Production* 23(7): 20-24.
30. Michaeli, W., and Korte, W. 1993. Better weld quality in ultrasonic welding — force control using Servovalve opens up new approaches of process control. *Kunststoffe* 83(96): 667-670.
31. Jagota, A., and Dawson, P. R. 1987. The influence of lateral wall vibrations on the ultrasonic welding of thin-walled parts. *J. of Engineering for Industry, Trans. ASME* 109(2): 140-147.
32. Franklin, G. 1995. Precision jointing with ultrasonic welding. *Materials World* 3(6): 279-280.
33. Johnson, N. 1998. Rapid Prototyping Using Metal Ultrasonic Welding. M.S. thesis. Department of Mechanical Engineering, Tufts University, Medford, Mass.
34. Gao, Y. 1999. Mechanical Analysis of Ultrasonic Metal Welding for Rapid Prototyping. M.S. thesis. Department of Mechanical En-

gineering, Tufts University, Medford, Mass.

35. Weare, N. E., Antonevich, J. N., and Monroe, R. E. 1960. Fundamental studies of ultrasonic welding. *Welding Journal* 39(8): 331-s to 341-s.
36. Golde, H. D. 1997. *Ultrasonic Metal Welding*. Landsberg, Germany: Verlag Moderne Industrie.
37. Yadav, S. 2001. Thermo-Mechanical Analysis of Ultrasonic Metal Welding. M.S. thesis. Department of Mechanical Engineering, Tufts University, Medford, Mass.
38. Timoshenko, S., and Young, D. H. 1968. *Elements of Strength of Materials*, 5th Edition. New York: Van Nostrand.
39. Persson, B. N. J. 1998. *Sliding Friction — Physical Principles and Applications*. Berlin-Heidelberg, Germany: Springer-Verlag.
40. SAS IP Inc. 1997. *ANSYS Theory Reference*. 8th Edition.
41. Meyers, M. A., Murr, L. E., and Staudhammer, K. P. 1992. *Shock-Wave and High-Strain-Rate Phenomena in Materials*. Reading, Mass.: M. Dekker.
42. Tani, J., Takagi, T., and Qiu, J. 1998. Intelligent material systems: applications of functional materials. *Trans. ASME Appl. Mechanics Reviews* 51(8): 505-521.

Change of Address? Moving?

Make sure delivery of your *Welding Journal* is not interrupted. Contact the Membership Department with your new address information — (800) 443-9353, ext. 480; jleon@aws.org.

REPRINTS REPRINTS

To order custom reprints
of articles in
Welding Journal,
call FosteReprints at
(219) 879-8366 or
(800) 382-0808 or.
Request for quotes can be
faxed to (219) 874-2849.
You can e-mail
FosteReprints at
sales@fostereprints.com